A hybrid procedure for cracking, creep, shrinkage and thermal gradient in continuous composite bridges

Sandeep Chaudhary[1], Umesh Pendharkar[2] and A.K. Nagpal[3,*]

[1]Deptt. of Structural Engg., Malaviya National Institute of Technology, Jaipur, India
[2]Deptt. of Civil Engg., Ujjain Engineering College, Ujjain, India
[3]Deptt. of Civil Engg., Indian Institute of Technology, Delhi, India

Abstract

A hybrid analytical-numerical procedure has been presented in this paper for the service load analysis of continuous composite bridges. The procedure accounts for the effects of concrete cracking, creep and shrinkage in the concrete portion and thermal gradient across the cross-section. The procedure is analytical at the elemental level and numerical at the structural level. A cracked span length beam element consisting of an uncracked zone in middle and cracked zones near the ends has been proposed to drastically reduce the computational effort. The progressive nature of cracking of concrete has been taken into account by division of the time into a number of time intervals. Closed form expressions for the stiffness matrix, end displacements, crack lengths, interpolation coefficients, and the mid-span deflection of the beam element have been presented in order to reduce the computational effort and the book-keeping. The procedure has been validated by comparison with the experimental and analytical results reported elsewhere and with FEM. The procedure can be readily extended for the analysis of integral composite bridges and three dimensional framed buildings.

1 Introduction

The composite beam is one of the economical forms of bridge construction. In continuous composite bridges, the time-dependent effects of creep and shrinkage in concrete can lead to the progressive cracking of concrete slab near interior supports and result in considerable moment redistribution along with increase in deflections. Bridges are directly exposed to sunlight and therefore a thermal gradient arises across the cross-section. In composite bridges, this can increase the tensile stresses [28] and thereby increase the cracking and mid-span deflections.

Extensive literature is available on time-dependent analysis of continuous composite beams up to ultimate load stage. Such procedures have been presented by Sakr and Lapos [27], Kwak and Seo [21], Kwak et al. [22, 23], Mari et al. [25] and Fragiacomo et al. [15]. The procedures take into account the progressive cracking. In these procedures, the division of the beam along

---

Notation

A, B, I	area, first moment of area and second moment of area respectively
E, L	modulus of elasticity and span length respectively
M	bending moment
$\{P\}, \{p\}$	force vector of composite beam and beam element respectively
$d_m, \{d\}$	mid-span deflection and displacement vector of beam element respectively
f_t	tensile strength of concrete
$f_{ij}, k_{ij}, [k]$	flexibility coefficients, stiffness coefficients and stiffness matrix of a beam element respectively
n	modular ratio
w	uniformly distributed load
x, y	crack length or distance from end A and $L - x$ respectively
β, λ	creep factor for curvature and strain respectively
$\varepsilon, \rho, \sigma$	top fiber strain, curvature and top fiber stress respectively
$\phi, \chi, \varepsilon^{sh}$	creep coefficient, aging coefficient and shrinkage strain respectively
α	coefficient of thermal expansion
θ	rotation
ξ, η	interpolation coefficient and 1- ξ respectively

Subscript

A, B	ends A and B respectively
c, s	concrete/concrete slab and steel respectively
cr, ts, un	cracked state/cracked section, tension stiffening and uncracked state/ uncracked transformed section respectively
e	age-adjusted
rs, ss	reinforcement and steel section respectively

Superscript

c, s, tm	creep, shrinkage and temperature respectively
cs	creep and shrinkage both
er	error or residual
id, it, t	indeterminate, instantaneous and total respectively

the length and across the section is required to take into account the non-linear behaviour under ultimate load but this division leads to considerable increase in the computational effort.

Some numerical procedures have been proposed for the time-dependent analysis of continuous composite beams under service load. A coupled system of equations has been proposed by Dezi and Tarantino [11] for inelastic analysis of continuous composite beams by discretising the time

into a number of time intervals. The beam has been considered to be uncracked and is discretised along its axis. Subsequently, the time-dependent analysis of prestressed continuous composite beams has also been proposed using the coupled system of equations [9]. Cracking is neglected in this method as it is assumed that prestressing is sufficient to prevent cracking. A simplification in the method has been proposed later on to carry out the analysis in a single time step [10].

A simplified analytical model using the closed form expressions has been presented to evaluate the creep and shrinkage effects in simply supported composite beams [2] neglecting the cracking. Another simple analytical procedure for the time-dependent analysis of two equal span continuous composite beams under service load, taking into account cracking, has been proposed by Gilbert and Bradford [18]. The transformed section approach has been used and the beam is taken as one element without subdivision along the length and across the cross-section. The analysis is carried out in single time step and the same crack lengths are assumed for the entire time interval beginning from the time of application of the load. The progressive nature of cracking i.e. continuous change in crack length of the beam with time is therefore not taken into account in this approach. Tension stiffening has also been neglected in the procedure. This analytical procedure has been further extended by Bradford et al. [7] making it applicable for two unequal span continuous composite beams. The effect of thermal gradient has not been considered in these procedures.

The above procedure [18] has been extended by Arockiasamy and Sivakumar [3], for the analysis of two span continuous composite integral bridges taking into account the thermal gradient. The above approach though convenient for two-span bridges, would tend to become tedious if extended to bridge having more than two spans. Simple close form expressions [19] for composite bridges with limited number of spans are available to ascertain if shrinkage and thermal gradient would result in subsequent cracking of initially uncracked beams.

On the other hand, elaborate approaches [15, 21–23, 25, 27] are though more general and accurate but their application for the analysis at service load [25] requires subdivision of the beams along the length and across the cross-section.

Therefore for application to continuous composite bridges, development of a procedure that requires a minimal computational effort and is yet accurate is desirable. Herein, for service load, a hybrid analytical-numerical procedure has been presented to take into account the effects of concrete cracking, creep, shrinkage and thermal gradient in continuous composite bridges. The procedure is analytical at the elemental level and numerical at the structural level. The cracked span length beam element consisting of an uncracked zone in the middle and cracked zones near the ends has been proposed. Closed form expressions for the stiffness matrix, end displacements, crack lengths, interpolation coefficients and mid-span deflection of the beam element have been presented. This approach drastically reduces the computational effort. The proposed procedure takes into account the progressive nature of cracking of concrete by division of the time into a number of time intervals. The tension stiffening effect has also been incorporated in the proposed procedure. The procedure has been validated by comparison with the experimental and analytical results [18] and with finite element method. The procedure can be readily extended

for analysis of integral composite bridges and three dimensional framed buildings.

2   Cross-section analysis

A typical composite cross-section along with the strain distribution is shown in Fig. 1. It is
assumed that a plane cross-section remains plane. Slip between the slab and the steel section
has been neglected since the earlier experiments and studies [5,6] have shown that the slip under
sustained service load can be neglected provided the shear connectors are at a sufficient close
spacing. The closer spacing is desirable from design considerations also, since this reduces the
deflections. Under service load, the stress-strain relationship of concrete, prior to cracking, is
assumed to be linearly elastic in both compression and tension. The concrete portion across
the cross-section is assumed to be completely cracked, when the top fiber stress of the concrete
slab exceeds the tensile strength of concrete, f_t, since the moment required for cracking the
slab fully is only slightly larger than the moment required for cracking the top fiber only [7].
It is further assumed that in the region of sagging moment, the effect of cracking if it occurs
is negligible [7, 26].The stress-strain relationship for steel in both tension and compression is
also assumed to be linear and stresses in steel section are assumed to be below the yield stress,
this would generally be the case when high strength steel sections are used. Since the neutral
axis varies with time and is also different for the cracked and the uncracked cross-sections, the
top fiber of the composite cross-section has been selected as the reference axis. Age-adjusted
effective modulus method [4] is used for predicting creep and shrinkage effects.
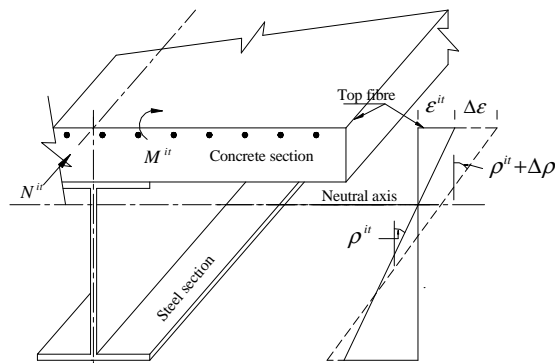
Figure 1: Composite cross-section and strain distribution.

The curvature, ρ^{it}, the instantaneous top fiber strain, ε^{it} and the instantaneous top fiber
stress, σ^{it} due to applied moment M^{it} and axial force N^{it} (the superscript, *it* here and subse-
quently in other quantities indicates the instantaneous value of the quantity), at a cross-section

(Fig. 1) are given as [17]

$$\rho^{it} = S^x M^{it} + S^{xy} N^{it} \tag{1}$$

$$\varepsilon^{it} = S^{xy} M^{it} + S^y N^{it} \tag{2}$$

$$\sigma^{it} = E_c \varepsilon^{it} \tag{3}$$

where, the quantities S^x, S^y and S^{xy} are given as

$$S^x = \frac{A}{E_c \left(AI - B^2 \right)} \tag{4}$$

$$S^y = \frac{I}{E_c \left(AI - B^2 \right)} \tag{5}$$

$$S^{xy} = \frac{B}{E_c \left(AI - B^2 \right)} \tag{6}$$

where E_c = modulus of elasticity of concrete; A = area of the transformed cross-section and B, I = first and second moment of area of the transformed cross-section about the reference axis. It may be noted that when the concrete portion across the cross-section is completely cracked, the properties of the cross-section are those of the transformed steel section and reinforcement in the slab only.

There is no axial force in continuous composite beams; therefore ρ^{it} and ε^{it} are given as

$$\rho^{it} = S^x M^{it} \tag{7}$$

$$\varepsilon^{it} = S^{xy} M^{it} \tag{8}$$

In an intermediate span of a continuous composite beam, there may be two cracked zones near the ends and an uncracked zone in the middle.

First consider a cross-section in the uncracked zone. Let the instantaneous curvature, the instantaneous top fiber strain, and the instantaneous top fiber stress be designated as ρ^{it}_{un}, ε^{it}_{un} and σ^{it}_{un} respectively (the subscript, un here and subsequently in other quantities indicates that the quantities are evaluated using transformed uncracked cross-sectional properties).

Consider now, the effect of creep in the cross-section. Assuming the concrete to be completely unrestrained, in a time interval beginning from the time of application of load, the change in curvature and the top fiber strain due to creep would be $\phi\rho^{it}_{un}$ and $\phi\varepsilon^{it}_{un}$ respectively where $\phi=$ creep coefficient at the end of the time interval. To restrain these changes, gradually applied bending moment $-\Delta M^c_{un}$ and axial force $-\Delta N^c_{un}$ (the superscript, c here and subsequently in other quantities indicates that these quantities arise from creep) are required. The quantities ΔM^c_{un} and ΔN^c_{un} are given as [17]

$$\Delta M^c_{un} = E_e \phi \left(-B_c \varepsilon^{it}_{un} + I_c \rho^{it}_{un} \right) \tag{9}$$

$$\Delta N^c_{un} = E_e \phi \left(A_c \varepsilon^{it}_{un} - B_c \rho^{it}_{un} \right) \tag{10}$$

where A_c = area of concrete; B_c and I_c = first moment of area and second moment of area of concrete about the top fiber and E_e= age-adjusted effective modulus of concrete given as $E_c/(1 + \chi\phi)$ in which χ = aging coefficient and may be assumed as 0.8 [7, 8, 18].

Equilibrium is restored by applying ΔM_{un}^c and ΔN_{un}^c on the cross-section. The changes, $\Delta\rho_{un}^c$ in the curvature, and $\Delta\varepsilon_{un}^c$ in the top fiber strain, due to ΔM_{un}^c and ΔN_{un}^c are obtained from Eqs. (1) and (2) respectively, on replacing M^{it} and N^{it} by ΔM_{un}^c and ΔN_{un}^c respectively and S^x, S^y and S^{xy} by $S_{e,un}^x$, $S_{e,un}^y$ and $S_{e,un}^{xy}$ (since ΔM_{un}^c, ΔN_{un}^c are developed gradually) respectively, and can be expressed in following form:

$$\Delta\rho_{un}^c = \beta_{un}^c \rho_{un}^{it} \tag{11}$$

$$\Delta\varepsilon_{un}^c = \lambda_{un}^c \varepsilon_{un}^{it} \tag{12}$$

$$\beta_{un}^c = (\phi E_e/A_{un}) \left(A_c B_{un} S_{e,un}^{xy} - B_c A_{un} S_{e,un}^{xy} - B_c B_{un} S_{e,un}^x + I_c A_{un} S_{e,un}^x \right) \tag{13}$$

$$\lambda_{un}^c = (\phi E_e/B_{un}) \left(A_c B_{un} S_{e,un}^y - B_c A_{un} S_{e,un}^y - B_c B_{un} S_{e,un}^{xy} + I_c A_{un} S_{e,un}^{xy} \right) \tag{14}$$

where $S_{e,un}^x$, $S_{e,un}^y$ and $S_{e,un}^{xy}$ are evaluated from Eqs. (4)-(6) on replacing A, B and I by the age-adjusted properties A_e, B_e and I_e respectively that in turn are evaluated using the age-adjusted modular ratio $n_e = E_s/E_e$ (E_s = modulus of elasticity of steel). It may be noted that β_{un}^c is the creep factor for the curvature by which the instantaneous curvature of an uncracked cross-section is to be multiplied to yield the change in curvature resulting from the creep. Similarly, λ_{un}^c is the creep factor for the strain.

Consider now, the effect of shrinkage in this cross-section. The changes, $\Delta\rho_{un}^s$ in the curvature and $\Delta\varepsilon_{un}^s$ in the top fiber strain (the superscript, s here and subsequently in other quantities indicates that the quantity arises from shrinkage), owing to shrinkage, are given as [17]

$$\Delta\rho_{un}^s = \varepsilon^{sh} E_e \left(S_{e,un}^{xy} A_c - S_{e,un}^x B_c \right) \tag{15}$$

$$\Delta\varepsilon_{un}^s = \varepsilon^{sh} E_e \left(S_{e,un}^y A_c - S_{e,un}^{xy} B_c \right) \tag{16}$$

where ε^{sh}= shrinkage strain at the end of the time interval.

Next, consider the thermal gradient. It varies continuously with time. A rigorous analysis would be computationally too expensive since short term variations of equivalent steady state temperature over a few days or few weeks need to be considered over a long period ($\simeq$30 years typically). Further, this data is generally not available. Therefore, it is a common practice to superimpose the thermal effects resulting from thermal gradients (positive or negative) at an instant of time on the time varying effects resulting from creep and shrinkage. In a manner described above for creep and shrinkage, first, the restraining forces ΔM_{un}^{tm} and ΔN_{un}^{tm} (the superscript, tm here and subsequently in other quantities indicates that the quantities arise from thermal gradient) are obtained by restraining the changes in curvature and strain of unrestrained concrete and steel. The curvature, $\Delta\rho_{un}^{tm}$ and strain, $\Delta\varepsilon_{un}^{tm}$ are then given by Eqs. (1) and (2)

respectively, on replacing M^{it} and N^{it} by ΔM_{un}^{tm} and ΔN_{un}^{tm} respectively. For a typical tri linear temperature profile {as adopted by AASHTO [1]} shown in Fig. 2 (a, b), the quantities ΔM_{un}^{tm} and ΔN_{un}^{tm} may be expressed as

$$
\begin{aligned}
\Delta M_{un}^{tm} = E_c \Big\{ &\alpha_c \left[B_c \left(T_1 - 2g_1 D_c/3 \right) + \Delta g \left(b_c/6 \right) \left(D_c - D^! \right)^2 \left(2D_c + D^! \right) \right] + \\
&\alpha_s \left[A_{sr} \left(n - \alpha_c/\alpha_s \right) T_{sr} D_{sr} + A_{ss} n T_3 D_{ss} \right] \Big\}
\end{aligned}
\tag{17}
$$

$$
\Delta N_{un}^{tm} = E_c \Big\{ \alpha_c \left[A_c \left(T_1 - g_1 D_c/2 \right) + \left(b_c/2 \right) \Delta g \left(D_c - D^! \right)^2 \right] + \alpha_s \left[A_{sr} \left(n - \alpha_c/\alpha_s \right) T_{sr} + A_{ss} n T_3 \right] \Big\}
\tag{18}
$$

where α_c, α_s=coefficient of thermal expansion of concrete and steel respectively; A_{sr}, A_{ss}=area of steel reinforcement and steel section respectively; T_{sr}=temperature at the level of steel reinforcement and $\Delta g = g_1 - g_2$.
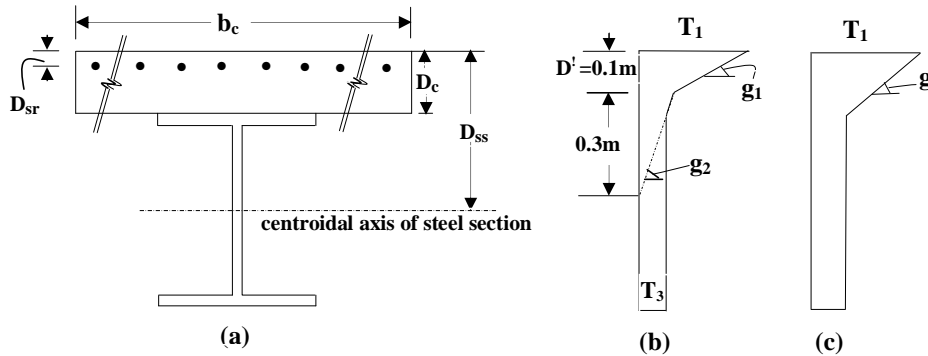
Figure 2: Typical thermal gradients for composite bridge cross-section: (a) cross-section; (b) trilinear gradient (AASHTO 1998); and (c) bilinear gradient.

For a bilinear profile [Fig. 2(a, c)] (as is the case for slabs upto 100 mm thick) and the same coefficient of thermal expansion, α for steel and concrete, the quantities $\Delta\rho_{un}^{tm}$ and $\Delta\varepsilon_{un}^{tm}$ may be explicitly expressed as

$$
\Delta\rho_{un}^{tm} = \alpha \left\{ -g + g E_s \left[S_{un}^x I_{ss} - S_{un}^{xy} B_{ss} + D_c \left(S_{un}^{xy} A_{ss} - S_{un}^x B_{ss} \right) \right] \right\}
\tag{19}
$$

$$
\Delta\varepsilon_{un}^{tm} = \alpha \left\{ -T_1 + g E_s \left[S_{un}^{xy} I_{ss} - S_{un}^y B_{ss} + D_c \left(S_{un}^y A_{ss} - S_{un}^{xy} B_{ss} \right) \right] \right\}
\tag{20}
$$

where B_{ss} and I_{ss} = first moment of area and second moment of area of steel section about the top fiber respectively.

In indeterminate structures, an additional moment $\Delta M^{id,cs}$ (the superscript, id, cs here and subsequently in other quantities indicates that the quantities arise in indeterminate structures gradually due to creep and shrinkage) is generated. The additional curvature, $\Delta\rho_{un}^{id,cs}$, the

additional top fiber strain, $\Delta\varepsilon_{un}^{id,cs}$ and the additional top fiber stress, $\Delta\sigma_{un}^{id,cs}$ due to $\Delta M^{id,cs}$ are given by Eqs. (7), (8) and (3) respectively on replacement of M^{it} by ΔM^{id} and E_c, S^x, S^y, S^{xy} by E_e, $S_{e,un}^x$, $S_{e,un}^y$, $S_{e,un}^{xy}$ respectively. Similarly, an additional moment $\Delta M^{id,tm}$ (the superscript, id, tm here and subsequently in other quantities indicates that the quantities arise in indeterminate structures at an instant of time due to thermal gradient) is also generated. The additional curvature, $\Delta\rho_{un}^{id,tm}$, the additional top fiber strain, $\Delta\varepsilon_{un}^{id,tm}$ and the additional top fiber stress, $\Delta\sigma_{un}^{id,tm}$ due to $\Delta M^{id,tm}$ are given by Eqs. (7), (8) and (3) respectively on replacement of M^{it} by $\Delta M^{id,tm}$.

The total curvature, ρ_{un}^t, the total top fiber strain, ε_{un}^t and the total top fiber stress, σ_{un}^t (the superscript, t in the quantities here and subsequently in other quantities, indicates the total value of quantity at the end of a time interval) of an uncracked cross-section at the end of the time interval are obtained by adding the changes in the quantities in the time interval to their instantaneous values respectively, as

$$\rho_{un}^t = \rho_{un}^{it} + \Delta\rho_{un}^c + \Delta\rho_{un}^s + \Delta\rho_{un}^{tm} + \Delta\rho_{un}^{id,cs} + \Delta\rho_{un}^{id,tm} \tag{21}$$

$$\varepsilon_{un}^t = \varepsilon_{un}^{it} + \Delta\varepsilon_{un}^c + \Delta\varepsilon_{un}^s + \Delta\varepsilon_{un}^{tm} + \Delta\varepsilon_{un}^{id,cs} + \Delta\varepsilon_{un}^{id,tm} \tag{22}$$

$$\sigma_{un}^t = \sigma_{un}^{it} + E_e(\Delta\varepsilon_{un}^c + \Delta\varepsilon_{un}^s - \phi\varepsilon_{un}^{it} - \varepsilon^{sh}) + E_c(\Delta\varepsilon_{un}^{tm} - \alpha T_1) + \Delta\sigma_{un}^{id,cs} + \Delta\sigma_{un}^{id,tm} \tag{23}$$

Next consider a cross-section in the cracked zone. The tension stiffening effect is taken into account by considering the cross-section in two states, uncracked and cracked. The cracked cross-section in the uncracked state has the same properties as that of the uncracked cross-section. In the cracked state, as stated earlier, the properties of the cross-section are those evaluated considering the steel section and reinforcement in the concrete slab only. The contribution of cracked state in the cross-section is represented by interpolation coefficient, ξ whereas the contribution of uncracked state is represented by $\eta\,(=1-\xi)$.

The interpolation coefficient is evaluated by the following expression, based on Eurocode-2 [14]

$$\xi = 1 - \kappa\,(f_t/\sigma_{un})^2 \tag{24}$$

where $\kappa = 1.0$ for initial loading and 0.5 for long term loads; $\sigma_{un} =$ the tensile stress in the reference axis to be evaluated from Eq. (3) assuming the cross-section to be in the uncracked state

The instantaneous curvature, ρ_{ts}^{it} and the instantaneous top fiber strain, ε_{ts}^{it} (the subscript, ts here and subsequently in other quantities indicates that the tension stiffening effect has been taken into account) of the cross-section are equal to $\eta\rho_{un}^{it} + \xi\rho_{cr}^{it}$ and $\eta\varepsilon_{un}^{it} + \xi\varepsilon_{cr}^{it}$ respectively (the subscript, cr here and subsequently in other quantities, indicates the cracked state of the cross-section). ρ_{cr}^{it} and ε_{cr}^{it} are evaluated from Eqs. (7) and (8) respectively, on using the cracked state properties.

Consider now, the effect of creep, shrinkage and thermal gradient in a cross-section in the cracked zone. In the uncracked state, the change in curvature and strain is evaluated in the same

manner as explained earlier for the uncracked zone [Eqs. (11)-(20)]. In the cracked state, no change in curvature and strain takes place owing to creep and shrinkage. However, the changes occur in the cracked state owing to thermal gradient and the indeterminate moments, $\Delta M^{id,cs}$ and $\Delta M^{id,tm}$. The changes, $\Delta \rho_{cr}^{tm}$ in curvature and $\Delta \varepsilon_{cr}^{tm}$ in the strain, owing to thermal gradient are given by Eqs. (19) and (20) respectively, on replacement of uncracked state properties by the cracked state properties. The additional curvature, $\Delta \rho_{cr}^{id,cs}$ and the additional top fiber strain, $\Delta \varepsilon_{cr}^{id,cs}$ due to $\Delta M^{id,cs}$ are given by Eqs. (1) and (2) respectively on replacement of M^{it} by $\Delta M^{id,cs}$ and using cracked state properties. Similarly, the additional curvature, $\Delta \rho_{cr}^{id,tm}$ and the additional top fiber strain, $\Delta \varepsilon_{cr}^{id,tm}$ due to $\Delta M^{id,tm}$ are given by Eqs. (1) and (2 respectively on replacement of M^{it} by $\Delta M^{id,tm}$ and using cracked state properties. The total curvature, ρ_{ts}^{t} and the total top fiber strain, ε_{ts}^{t} of a cross-section in the cracked zone, at the end of the time interval are obtained by adding the changes in the uncracked and the cracked state of cross-section to the instantaneous values and are given as

$$\rho_{ts}^{t} = \eta \left(\rho_{un}^{it} + \Delta\rho_{un}^{c} + \Delta\rho_{un}^{s} + \Delta\rho_{un}^{tm} + \Delta\rho_{un}^{id,cs} + \Delta\rho_{un}^{id,tm} \right) + \xi(\rho_{cr}^{it} + \Delta\rho_{cr}^{tm} + \Delta\rho_{cr}^{id,cs} + \Delta\rho_{cr}^{id,tm})$$
(25)

$$\varepsilon_{ts}^{t} = \eta \left(\varepsilon_{un}^{it} + \Delta\varepsilon_{un}^{c} + \Delta\varepsilon_{un}^{s} + \Delta\varepsilon_{un}^{tm} + \Delta\varepsilon_{un}^{id,cs} + \Delta\varepsilon_{un}^{id,tm} \right) + \xi \left(\varepsilon_{cr}^{it} + \Delta\varepsilon_{cr}^{tm} + \Delta\varepsilon_{cr}^{id,cs} + \Delta\varepsilon_{cr}^{id,tm} \right)$$
(26)

The total moment, M^{t} at the end of a time interval, at a cross-section, in both the uncracked and cracked zones is expressed as, $M^{t} = M^{it} + \Delta M^{id,cs} + \Delta M^{id,tm}$.

3   Cracked span length beam element

In a typical continuous beam of a composite bridge, cracks would occur near interior supports if the tensile stress in the top fiber of a cross-section exceeds the tensile strength of concrete. A typical cracked span length beam element therefore consists of three zones, two cracked zones of length x_A, x_B, near ends A and B respectively, and an uncracked zone in the middle [Fig. 3(a)]. For a completely cracked beam element, x_A and x_B would be equal to $L/2$.

The stiffness matrix and the load vector of a cracked span length beam element are of interest. In order to evaluate these, releases 1 and 2 are introduced at the ends [Fig. 3(b)]. For the evaluation of stiffness matrix, the flexibility coefficients $f_{11}, f_{12}, f_{21}, f_{22}$ that are required can be found by the principle of virtual work using m_A and m_B diagrams (Fig. 4), as

$$f_{11} = \int_0^L S^x m_A^2 dx \tag{27}$$

$$f_{12} = f_{21} = \int_0^L S^x m_A m_B dx \tag{28}$$

$$f_{22} = \int_0^L S^x m_A^2 dx \tag{29}$$

Eqs. (27)-(29) are to be integrated for the uncracked zone and the two cracked zones. For a cross-section in the uncracked zone, S^x is replaced by S_{un}^x whereas for a cross-section in a cracked zone, considering the tension stiffening effect, S^x is to be replaced by $\xi S_{cr}^x + \eta S_{un}^x$.
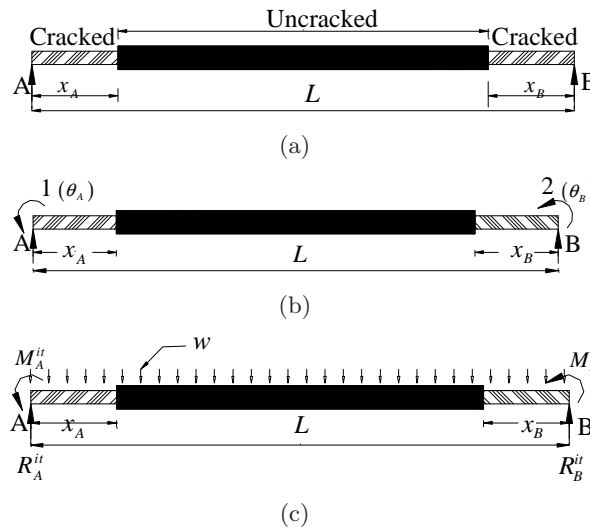
Figure 3: Cracked span length beam element: (a) zones; (b) degrees of freedom and releases; and (c) loading and end forces.

A single interpolation coefficient has been assumed for each cracked zone. The interpolation coefficient for cracked zones near ends A and B are termed as ξ_A and ξ_B respectively and are evaluated from Eq. (13) in which σ_{un} is replaced by the representative stresses, $\sigma_{un,A}$ and $\sigma_{un,B}$ respectively that are obtained by dividing the area of stress diagrams σ_{un} over crack lengths x_A and x_B respectively by respective crack lengths x_A and x_B. The closed form expressions for f_{11}, f_{12}, f_{21} and f_{22} obtained from Eqs. (27)-(29), incorporating the tension stiffening effect, are given as

$$f_{11} = \left(1/3L^2\right)\left[S_{un}^x \left(\eta_A L^3 - \xi_B x_B^3 + \xi_A y_A^3\right) + S_{cr}^x \left(\xi_A L^3 + \xi_B x_B^3 - \xi_A y_A^3\right)\right] \tag{30}$$

$$f_{12} = f_{21} = \left(1/6L^2\right)\left[\xi_A x_A^2 \left(2x_A - 3L\right) + \xi_B x_B^2 \left(2x_B - 3L\right)\right]\left(S_{cr}^x - S_{un}^x\right) - \left(S_{un}^x L/6\right) \tag{31}$$
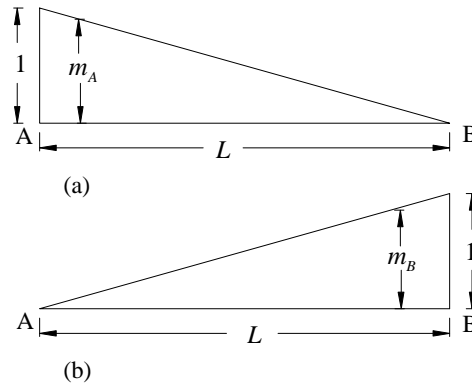
Figure 4: (a) m_A diagram; and (b) m_B diagram.

$$f_{22} = \left(1/3L^2\right)\left[S_{un}^x\left(\eta_B L^3 - \xi_A x_A^3 + \xi_B y_B^3\right) + S_{cr}^x\left(\xi_B L^3 + \xi_A x_A^3 - \xi_B y_B^3\right)\right] \tag{32}$$

Stiffness matrix, $[k]$ is the inverse of flexibility matrix and the stiffness matrix coefficients, k_{11}, k_{12}, k_{21} and k_{22} may be expressed in the closed form as

$$k_{11} = f_{22}/(f_{11}f_{22} - f_{21}f_{12}) \tag{33}$$

$$k_{12} = k_{21} = -f_{12}/(f_{11}f_{22} - f_{21}f_{12}) \tag{34}$$

$$k_{22} = f_{11}/(f_{11}f_{22} - f_{21}f_{12}) \tag{35}$$

For evaluation of the fixed end moments, additionally the rotations at the ends are required. The end rotations of the released beam element due to applied vertical load, and creep and shrinkage are found by integrating m_A and m_B diagrams (Fig. 4) respectively with the corresponding curvature diagram.

For a beam element, subjected to uniformly distributed span load, w and also additionally the instantaneous moments M_A^{it} and M_B^{it} at the ends A and B respectively [Fig. 3(c)], the instantaneous rotations θ_A^{it} and θ_B^{it} may be expressed in the closed form, on integrating m_A and m_B diagrams (Fig. 4) respectively with $\rho^{it}(x)$, which is obtained from Eq. (7) on substitution of M^{it} by $R_B^{it}x + M_B^{it} - wx^2/2$ and $R_A^{it}x - M_A^{it} - wx^2/2$ respectively where R_A^{it} and $R_B^{it} =$ the instantaneous reactions at the ends A and B respectively and $x =$ distance of cross-section from end B for θ_A^{it} and from end A for θ_B^{it}. The expressions for θ_A^{it} and θ_B^{it} are obtained as

$$
\begin{aligned}
\theta_A^{it} = (1/24L)\Big\{ & S_{un}^x\left[-8R_B^{it}\left(\eta_A L^3 + \xi_A y_A^3 - \xi_B x_B^3\right) + 3w\left(\eta_A L^4 + \xi_A y_A^4 - \xi_B x_B^4\right)\right. \\
& \left. -12M_B^{it}\left(\eta_A L^2 + \xi_A y_A^2 - \xi_B x_B^2\right)\right] + S_{cr}^x\left[-8R_B^{it}\left(\xi_A L^3 - \xi_A y_A^3 + \xi_B x_B^3\right)\right. \\
& \left. + 3w\left(\xi_A L^4 - \xi_A y_A^4 + \xi_B x_B^4\right) - 12M_B^{it}\left(\xi_A L^2 - \xi_A y_A^2 + \xi_B x_B^2\right)\right]\Big\}
\end{aligned}
\tag{36}
$$

$$\theta_B^{it} = (1/24L) \left\{ S_{un}^x \left[8R_A^{it} \left(\eta_B L^3 + \xi_B y_B^3 - \xi_A x_A^3 \right) - 3w \left(\eta_B L^4 + \xi_B y_B^4 - \xi_A x_A^4 \right) \right. \right.$$
$$\left. -12M_A^{it} \left(\eta_B L^2 + \xi_B y_B^2 - \xi_A x_A^2 \right) \right] + S_{cr}^x \left[8R_A^{it} \left(\xi_B L^3 - \xi_B y_B^3 + \xi_A x_A^3 \right) \right.$$
$$\left. \left. -3w \left(\xi_B L^4 - \xi_B y_B^4 + \xi_A x_A^4 \right) - 12M_A^{it} \left(\xi_B L^2 - \xi_B y_B^2 + \xi_A x_A^2 \right) \right] \right\} \quad (37)$$

The first terms in Eqs. (36) and (37) are the contributions of the uncracked zone and the uncracked state of the cracked zone whereas the second terms are the contributions of the cracked state of the cracked zone.

The mid-span deflection, d_m of a beam element is also of interest and may be expressed as [13]:

$$d_m = (1/2) \int_0^{L/2} \rho(x) x \, dx + (L/2) \int_{L/2}^L \rho(x) \left(1 - x/L \right) dx \quad (38)$$

For the beam element shown in Fig. 3(c), instantaneous mid-span deflection d_m^{it} may be expressed in the closed form, on replacing $\rho(x)$ by $\rho^{it}(x)$, as

$$d_m^{it} = (1/384) \left\{ 8 \left(S_{cr}^x - S_{un}^x \right) \left[\xi_A \left(8R_A^{it} x_A^3 - 12M_A^{it} x_A^2 - 3w x_A^4 \right) + \xi_B \left(8R_B^{it} x_B^3 + 12M_B^{it} x_B^2 - 3w x_B^4 \right) \right] \right.$$
$$\left. + S_{un}^x L^2 \left[24(M_B^{it} - M_A^{it}) + 5w L^2 \right] \right\}$$
$$(39)$$

Creep in the concrete increases the curvature of the uncracked zone and the uncracked state of the cracked zone by a factor β_{un}^c [Eq. (5)] which leads to the changes, $\Delta \theta_A^c$ and $\Delta \theta_B^c$ in the end rotations if the ends are not restrained against the rotation. Since the creep does not take place in the cracked state, the rotations $\Delta \theta_A^c$ and $\Delta \theta_B^c$ can be expressed from Eqs. (36) and (37) respectively on dropping the second terms involving the cracked state and multiplying the remaining terms by β_{un}^c, as

$$\Delta \theta_A^c = (\beta_{un}^c S_{un}^x / 24L) \left[-8R_B^{it} \left(\eta_A L^3 + \xi_A y_A^3 - \xi_B x_B^3 \right) + 3w \left(\eta_A L^4 + \xi_A y_A^4 - \xi_B x_B^4 \right) \right.$$
$$\left. -12M_B^{it} \left(\eta_A L^2 + \xi_A y_A^2 - \xi_B x_B^2 \right) \right] \quad (40)$$

$$\Delta \theta_B^c = (\beta_{un}^c S_{un}^x / 24L) \left[8R_A^{it} \left(\eta_B L^3 + \xi_B y_B^3 - \xi_A x_A^3 \right) - 3w \left(\eta_B L^4 + \xi_B y_B^4 - \xi_A x_A^4 \right) \right.$$
$$\left. -12M_A^{it} \left(\eta_B L^2 + \xi_B y_B^2 - \xi_A x_A^2 \right) \right] \quad (41)$$

The change in mid-span deflection, Δd_m^c owing to creep can also be expressed similarly from Eq. (38), as

$$\Delta d_m^c = (\beta_{un}^{c,m} S_{un}^x / 384) \left\{ 8 \left[-\xi_A \left(8R_A^{it} x_A^3 - 12M_A^{it} x_A^2 - 3w x_A^4 \right) - \xi_B \left(8R_B^{it} x_B^3 + 12M_B^{it} x_B^2 - 3w x_B^4 \right) \right] \right.$$
$$\left. + L^2 \left[24(M_B^{it} - M_A^{it}) + 5w L^2 \right] \right\} \quad (42)$$

The changes, $\Delta \theta_A^s$ and $\Delta \theta_B^s$ in the end rotations of the released beam element, owing to shrinkage, may be expressed in the closed from, on integrating m_A diagram and m_B diagram

with the curvature diagram due to shrinkage $\{\Delta\rho_{un}^s$ [Eq. (15)] for the uncracked zone and $\eta\Delta\rho_{un}^s$ for the cracked zone} respectively, as

$$\Delta\theta_A^s = (\Delta\rho_{un}^s/2L)\left(\xi_B x_B^2 - \xi_A y_A^2 - \eta_A L^2\right) \tag{43}$$

$$\Delta\theta_B^s = (\Delta\rho_{un}^s/2L)\left(\eta_B L^2 - \xi_A x_A^2 + \xi_B y_B^2\right) \tag{44}$$

Similarly, the change in mid-span deflection due to shrinkage, Δd_m^s may be expressed in the closed form from Eq. (38), on replacing $\rho(x)$ by $\Delta\rho_{un}^s$ for the uncracked zone and by $\eta\Delta\rho_{un}^s$ for the cracked zone, as

$$\Delta d_m^s = (\Delta\rho_{un}^s/\ 8)\left(L^2 - 2\xi_A x_A^2 - 2\xi_B x_B^2\right) \tag{45}$$

The changes, $\Delta\theta_A^{tm}$ and $\Delta\theta_B^{tm}$ in the end rotations of the released beam element, owing to thermal gradient, may be expressed in the closed from, on integrating m_A diagram and m_B diagram with the curvature diagram due to thermal gradient ($\Delta\rho_{un}^{tm}$ for the uncracked zone and $\eta\Delta\rho_{un}^{tm} + \xi\Delta\rho_{cr}^{tm}$ for the cracked zone) respectively, as

$$\Delta\theta_A^{tm} = (1/2L)\left[\Delta\rho_{un}^{tm}\left(\xi_B x_B^2 - \xi_A y_A^2 - \eta_A L^2\right) + \Delta\rho_{cr}^{tm}\left(\xi_A y_A^2 - \xi_B x_B^2 - \xi_A L^2\right)\right] \tag{46}$$

$$\Delta\theta_B^{tm} = (1/2L)\left[\Delta\rho_{un}^{tm}\left(\xi_B y_B^2 + \eta_B L^2 - \xi_A x_A^2\right) + \Delta\rho_{cr}^{tm}\left(\xi_A x_A^2 + \xi_B L^2 - \xi_B y_B^2\right)\right] \tag{47}$$

Similarly, the change in mid-span deflection due to thermal gradient, Δd_m^{tm} may be expressed in the closed form from Eq. (38), on replacing $\rho(x)$ by $\Delta\rho_{un}^{tm}$ for the uncracked zone and by $\eta\Delta\rho_{un}^{tm} + \xi\Delta\rho_{cr}^{tm}$ for the cracked zone, as

$$\Delta d_m^{tm} = (1/\ 8)\left[2\left(\Delta\rho_{cr}^{tm} - \Delta\rho_{un}^{tm}\right)\left(\xi_A x_A^2 + \xi_B x_B^2\right) + \Delta\rho_{un}^{tm}L^2\right] \tag{48}$$

The closed form expression for $\Delta d_m^{id,cs}$, the additional mid-span deflection due to $\Delta M^{id,cs}$, may be obtained from Eq. (39), on dropping the terms involving w, on replacing M_A^{it}, M_B^{it}, R_A^{it} and R_B^{it} by $\Delta M_A^{id,cs}$, $\Delta M_B^{id,cs}$, $\Delta R_A^{id,cs}$ and $\Delta R_B^{id,cs}$ (the changes in end forces resulting from creep and shrinkage) respectively and S_{un}^x by $S_{e,un}^x$, as

$$\Delta d_m^{id,cs} = (1/48)\left\{\left(S_{cr}^x - S_{e,un}^x\right)\left[8\left(\xi_A\Delta R_A^{id,cs}x_A^3 + \xi_B\Delta R_B^{id,cs}x_B^3\right)\right.\right.$$
$$\left.\left. +12\left(-\xi_A\Delta M_A^{id,cs}x_A^2 + \xi_B\Delta M_B^{id,cs}x_B^2\right)\right] + 3S_{e,un}^x L^2\left(\Delta M_B^{id,cs} - \Delta M_A^{id,cs}\right)\right\} \tag{49}$$

Similarly, the closed form expression for $\Delta d_m^{id,tm}$, the additional mid-span deflection due to $\Delta M^{id,tm}$, may be obtained from Eq. (39) as

$$\Delta d_m^{id,tm} = (1/48)\left\{\left(S_{cr}^x - S_{un}^x\right)\left[8\left(\xi_A\Delta R_A^{id,tm}x_A^3 + \xi_B\Delta R_B^{id,tm}x_B^3\right)\right.\right.$$
$$\left.\left. +12\left(-\xi_A\Delta M_A^{id,tm}x_A^2 + \xi_B\Delta M_B^{id,tm}x_B^2\right)\right] + 3S_{un}^x L^2\left(\Delta M_B^{id,tm} - \Delta M_A^{id,tm}\right)\right\} \tag{50}$$

The total mid-span deflection, d_m^t at end of a time interval (beginning from the time of application of load) consists of d_m^{it}, Δd_m^c, Δd_m^s, $\Delta d_m^{id,cs}$ and $\Delta d_m^{id,tm}$ and may be expressed as

$$d_m^t = d_m^{it} + \Delta d_m^c + \Delta d_m^s + \Delta d_m^{id,cs} + \Delta d_m^{id,tm} \tag{51}$$

4 Analysis of a continuous beam of a composite bridge

The analysis of the continuous beam of composite bridge is carried out in two parts. In the first part, instantaneous analysis is carried out using an iterative method [16] to establish the instantaneous crack lengths. In the second part, time-dependent analysis is carried out by dividing the time into a number of time intervals. The cracked span length beam elements along with the closed form expressions are used in both the parts.

4.1 Instantaneous analysis

An iterative process is required to establish the instantaneous crack lengths, interpolation coefficients and moments at time t_1, the time of application of load. For a typical iterative cycle, a displacement analysis is carried out for the residual force vector, $\{P^{er}(t_1)\}$ (in which, here and subsequently for other quantities having one term in the parentheses, the term indicates the time instant at which the quantity is evaluated or assumed to arise) of the composite beam. The revised force vector, $\{p^{it}(t_1)\}$ $\left(\{p^{it}(t_1)\}^T = \{M_A^{it}(t_1),\ M_B^{it}(t_1)\}\right)$, and the revised displacement vector of the beam elements [Fig. 3(c)], $\{d^{it,*}(t_1)\}$ $\left(\{d^{it,*}(t_1)\}^T = \left\{\theta_A^{it,*}(t_1),\ \theta_B^{it,*}(t_1)\right\}\right)$ are obtained by adding the force vector and displacement vectors of this analysis to the force vector and displacement vector at the end of previous cycle.

Based on the revised force vector, $\{p^{it}(t_1)\}$, the revised crack lengths of beam elements, $x_A(t_1)$, $x_B(t_1)$ are established by locating the section at which the tensile stress in the top fiber, $\sigma_{un}^{it}(t_1)$ is equal to the tensile strength of concrete, $f_t(t_1)$. For the beam element shown in Fig. 3(c), the stress $\sigma_{un}^{it}(t_1)$ for a cross-section at distance x from end A is obtained from Eqs. (3) and (8), on substitution of $M^{it}(t_1)$ by $R_A^{it}(t_1)x - M_A^{it}(t_1) - wx^2/2$, as

$$\sigma_{un}^{it}(t_1) = a(t_1)x^2 + b(t_1)x + c(t_1) \tag{52}$$

where

$$a(t_1) = -0.5S_{un}^{xy}(t_1)E_c(t_1)w$$
$$b(t_1) = S_{un}^{xy}(t_1)E_c(t_1)R_A^{it}(t_1)$$
$$c(t_1) = -S_{un}^{xy}(t_1)E_c(t_1)M_A^{it}(t_1)$$

The crack lengths $x_A(t_1)$, $x_B(t_1)$ can now be expressed in the closed form, on equating $\sigma_{un}^{it}(t_1)$ with $f_t(t_1)$, as

$$x_A(t_1) = \frac{-b(t_1) + \sqrt{[b(t_1)]^2 - 4a(t_1)[c(t_1) - f_t(t_1)]}}{2a(t_1)} \tag{53}$$

$$x_B(t_1) = L + \frac{b(t_1) + \sqrt{[b(t_1)]^2 - 4a(t_1)[c(t_1) - f_t(t_1)]}}{2a(t_1)} \tag{54}$$

The interpolation coefficients $\xi_A(t_1)$ and $\xi_B(t_1)$ are obtained in a manner similar to that stated in section 3 using Eq. (52) as ($\kappa=1.0$)

$$\xi_A(t_1) = 1 - \kappa \left(\frac{6f_t(t_1)}{2a(t_1)\,x_A(t_1)^2 + 3b(t_1)\,x_A(t_1) + 6c(t_1)} \right)^2 \tag{55}$$

$$\xi_B(t_1) = 1 - \kappa \left(\frac{6x_B(t_1)f_t(t_1)}{2a(t_1)\left(L^3 - y_B(t_1)^3\right) + 3b(t_1)\left(L^2 - y_B(t_1)^2\right) + 6c(t_1)\,x_B(t_1)} \right)^2 \tag{56}$$

Changes in crack lengths and thereby end displacements of the composite beam element lead to the difference between the displacement vector, $\{d^{it,*}(t_1)\}$ and the displacement vector based on integration of curvature and strain.

The error $\{d^{er}(t_1)\}$ (or difference) in displacement vector, corresponding to releases 1, 2 is now given as $\{d^{er}(t_1)\}^T = \left\{ \theta_A^{it}(t_1) - \theta_A^{it,*}(t_1); \ \ \theta_B^{it}(t_1) - \theta_B^{it,*}(t_1) \right\}$ where the displacements $\theta_A^{it}(t_1)$ and $\theta_B^{it}(t_1)$ are obtained from Eqs. (36) and (37) respectively. The terms of residual force vector, $\{p^{er}(t_1)\}$, corresponding to this difference in displacement vector are given as $-[k(t_1)]\{d^{er}(t_1)\}$ where the terms of $[k(t_1)]$ are obtained from Eqs. (33)-(35).

The residual force vector, $\{p^{er}(t_1)\}$ of the beam elements are assembled to form the residual force vector, $\{P^{er}(t_1)\}$ of the composite beam. $\{P^{er}(t_1)\}$ should be within some permissible limit [16] for the iterative process to terminate, typically $\{P^{er}(t_1)\}^T\{P^{er}(t_1)\} \leq 0.001\{P^o(t_1)\}^T\{P^o(t_1)\}$, where $\{P^o(t_1)\}=$ fixed end force vector of the composite beam for first iteration (uncracked beam elements). Otherwise a new cycle is started.

4.2 Time-dependent analysis

The progressive nature of cracking in a continuous beam of a composite bridge with time is shown in Fig. 5. This results in change in creep and shrinkage characteristics of the beam with time. In order to account for these changes with time, the time-dependent analysis is carried out by dividing the time into a number of time intervals. In a time interval, the crack lengths are assumed to be constant and equal to that at the beginning of the time interval (Fig. 5). The moments, $\Delta M^{id,cs}$ and the change in instantaneous bending moment, ΔM^{it} (resulting from the change in crack length) are assumed to arise at the specified instants of time $t_1, t_{2,------}, t_j$ (Fig. 6) for considering their contributions to creep. In order to have common notation for the instantaneous analysis and the time-dependent analysis, $M^{it}(t_1)$ is redesignated as $\Delta M^{it}(t_1)$ and the instantaneous curvature, instantaneous top fiber strain, instantaneous top fiber stress at time t_1 are designated as $\Delta\rho^{it}(t_1), \Delta\varepsilon^{it}(t_1), \Delta\sigma^{it}(t_1)$ respectively.

The displacement method has been used for the time-dependent analysis also in which the fixed end forces owing to creep, shrinkage and thermal gradient and stiffness matrix of a beam element for a time interval are required.

Consider the first time interval (t_1, t_2). For the evaluation of the fixed end forces and the stiffness matrix, the cracked span length released beam element is considered. Owing to the creep
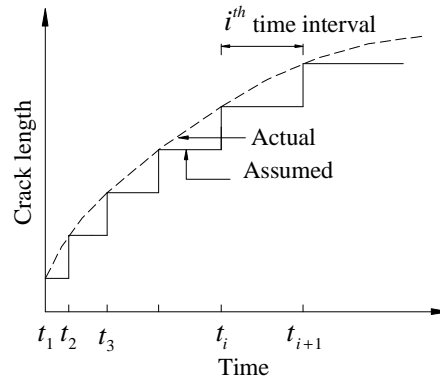
Figure 5: Progressive nature of cracking.
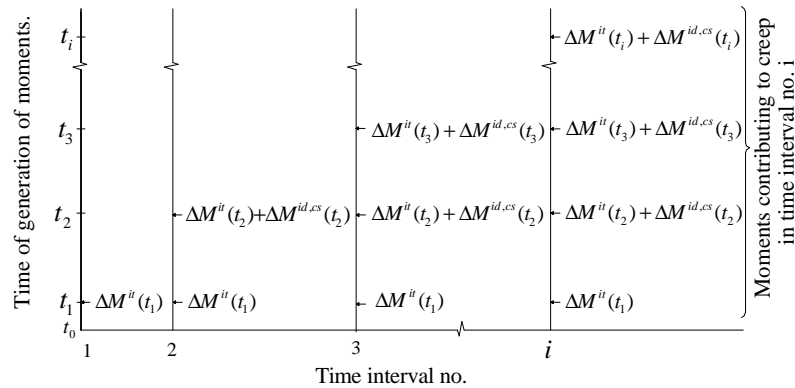
Figure 6: Time history of generation of moments contributing to creep.

in the cross-section of uncracked zone and uncracked state of the cracked zone, the curvature $\Delta\rho_{un}^{it}(t_1)$ changes by a factor $\Delta\beta_{un}^{c}(t_2,t_1,t_1)$ [see Eq. (11)], leading to the change in curvature $\Delta\rho_{un}^{c}(t_2,t_1,t_1)\left[=\Delta\rho_{un}^{it}(t_1)\Delta\beta_{un}^{c}(t_2,t_1,t_1)\right]$ in which, here and subsequently for other quantities having three terms in the parentheses, the first and second terms indicate the time of the end and the beginning of the interval (for which the change in a quantity is evaluated) respectively and the third term indicates the time of initiation of a cause from which the change arises. The cause may be either application of a moment or the shrinkage. Presently the quantity is the curvature and cause is the application of the moment $\Delta M^{it}(t_1)$. The factor $\Delta\beta_{un}^{c}(t_2,t_1,t_1)$ is given as $\beta_{un}^{c}(t_2,t_1) - \beta_{un}^{c}(t_1,t_1)$ in which, here and subsequently for other quantities having two terms in the parentheses, the first term indicates the time instant at which a quantity is evaluated whereas the second term indicates the time of initiation of the cause owing to which the quantity arises. The cause may be either application of the moment or shrinkage or gradual application of unit load (required for evaluation of age-adjusted flexibility matrix and hence

stiffness matrix) or application of stress (required for evaluating E_e). The factor $\beta_{un}^c(t_2, t_1)$ is evaluated from Eq. (13) in which ϕ is replaced by $\phi(t_2, t_1)$ and the age-adjusted cross-sectional properties are evaluated using the modular ratio $E_s/E_e(t_2, t_1)$. In turn, $E_e(t_2, t_1)$ is evaluated using $\phi(t_2, t_1)$ and $\chi(t_2, t_1)$. It may be noted that $\beta_{un}^c(t_1, t_1)=0$. As stated earlier, in the cracked zone there is no change in curvature of the cross- section in the cracked state. The changes in the rotations of the released beam element at end A, $\Delta\theta_A^c(t_2, t_1, t_1)$ and at end B, $\Delta\theta_B^c(t_2, t_1, t_1)$ resulting from $\Delta\rho_{un}^c(t_2, t_1, t_1)$ are evaluated from Eqs. (40) and (41) respectively in which β_{un}^c is replaced by $\Delta\beta_{un}^c(t_2, t_1, t_1)$.

Shrinkage is assumed to start from time t_1, the time of application of first load. Owing to the shrinkage, the change in curvature, $\Delta\rho_{un}^s(t_2, t_1, t_1)$ of a cross-section of uncracked zone and the uncracked state of the cracked zone is given as $\Delta\rho_{un}^s(t_2, t_1) - \Delta\rho_{un}^s(t_1, t_1)$. The quantity $\Delta\rho_{un}^s(t_2, t_1)$ is evaluated from Eq. (19) on replacing ε^{sh} by $\varepsilon^{sh}(t_2, t_1)$ and the age-adjusted properties are used in a manner similar to that described earlier for $\beta_{un}^c(t_2, t_1)$. Here again, it may be noted that $\Delta\rho_{un}^s(t_1, t_1) = 0$ and also that, in the cracked zone there is no change in curvature of the cross-section in the cracked state. Changes in the end rotations of the released beam, $\Delta\theta_A^s(t_2, t_1, t_1)$, $\Delta\theta_B^s(t_2, t_1, t_1)$ resulting from $\Delta\rho_{un}^s(t_2, t_1, t_1)$ are evaluated from Eqs. (43) and (44) respectively in which $\Delta\rho_{un}^s$ is replaced by $\Delta\rho_{un}^s(t_2, t_1, t_1)$.

The end displacements vector, $\{d^{cs}(t_2, t_1)\}$ of the released beam element due to creep and shrinkage in first time interval is now given as

$$\{d^{cs}(t_2, t_1)\}^T = \{\Delta\theta_A^c(t_2, t_1, t_1) + \Delta\theta_A^s(t_2, t_1, t_1); \; \Delta\theta_B^c(t_2, t_1, t_1) + \Delta\theta_B^s(t_2, t_1, t_1)\} \quad (57)$$

The vector of fixed end forces required to restrain these changes in end rotations is given as $-[k_e(t_2, t_1)]\{d^{cs}(t_2, t_1)\}$ where $[k_e(t_2, t_1)]$ is age-adjusted stiffness matrix and its terms are evaluated from Eqs. (33)-(35) using the age-adjusted cross-sectional properties. These vectors of fixed end forces of beam elements are assembled and a displacement analysis is carried out using the age-adjusted stiffness matrices. This displacement analysis leads to the moment, $\Delta M^{id,cs}(t_2)$ at a section.

Consider now the thermal gradient (positive or negative) acting at the end of the time interval. The changes $\Delta\theta_A^{tm}(t_2)$, $\Delta\theta_B^{tm}(t_2)$ in the end rotations of the released beam element are evaluated from Eqs. (46) and (47) respectively on replacing $\Delta\rho_{un}^{tm}$ and $\Delta\rho_{cr}^{tm}$ by $\Delta\rho_{un}^{tm}(t_2)$ and $\Delta\rho_{cr}^{tm}(t_2)$ respectively which may be obtained as explained in section 2. The vector of fixed end forces required to restrain these changes in end rotations is given as $-[k(t_2)]\{d^{tm}(t_2)\}$, where $d^{tm}(t_2)$ is given as

$$\{d^{tm}(t_2)\}^T = \{\Delta\theta_A^{tm}(t_2); \; \Delta\theta_B^{tm}(t_2)\} \quad (58)$$

These vectors of fixed end forces of beam elements are assembled and a displacement analysis is carried out using the age-adjusted stiffness matrices. This displacement analysis leads to the moment, $\Delta M^{id,tm}(t_2)$ at a section.

The total bending moment, $M^t(t_2)$ at a cross-section of a beam element at the end of first

time interval is given as

$$M^t(t_2) = \Delta M^{it}(t_1) + \Delta M^{id,cs}(t_2) + \Delta M^{id,tm}(t_2) \tag{59}$$

The deflection at mid-span of a beam element, $d_m^t(t_2)$ at the end of the first time interval is obtained from Eq. (27), as

$$d_m^t(t_2) = \Delta d_m^{it}(t_1) + \Delta d_m^c(t_2, t_1, t_1) + \Delta d_m^s(t_2, t_1, t_1) + \Delta d_m^{tm}(t_2) + \Delta d_m^{id,cs}(t_2) + \Delta d_m^{id,tm}(t_2) \tag{60}$$

where $\Delta d_m^{it}(t_1)(=d_m^{it})$, $\Delta d_m^c(t_2, t_1, t_1)(=\Delta d_m^c)$, $\Delta d_m^s(t_2, t_1, t_1)(=\Delta d_m^s)$ and $\Delta d_m^{id,cs}(t_2)(=\Delta d_m^{id})$ are obtained from Eqs. (39), (42), (45) and (49) respectively on replacing S_{un}^x, $S_{e,un}^x$, x_A, x_B, ξ_A, ξ_B, M_A^{it}, M_B^{it}, R_A^{it}, R_B^{it}, $\Delta M_A^{id,cs}$, $\Delta M_B^{id,cs}$, $\Delta R_A^{id,cs}$ and $\Delta R_B^{id,cs}$ by $S_{un}^x(t_1)$, $S_{e,un}^x(t_2, t_1)$, $x_A(t_1)$, $x_B(t_1)$, $\xi_A(t_1)$, $\xi_B(t_1)$, $\Delta M_A^{it}(t_1)$, $\Delta M_B^{it}(t_1)$, $\Delta R_A^{it}(t_1)$, $\Delta R_B^{it}(t_1)$, $\Delta M_A^{id,cs}(t_2)$, $\Delta M_B^{id,cs}(t_2)$, $\Delta R_A^{id,cs}(t_2)$ and $\Delta R_B^{id,cs}(t_2)$ respectively and β_{un}^c and $\Delta \rho_{un}^s$ by $\Delta \beta_{un}^c(t_2, t_1, t_1)$ and $\Delta \rho_{un}^s(t_2, t_1, t_1)$ respectively. The quantities $\Delta d_m^{tm}(t_2)(=\Delta d_m^{tm})$ and $\Delta d_m^{id,tm}(t_2)(=\Delta d_m^{id,tm})$ are obtained from Eq (48) and (50) respectively on replacing S_{un}^x, x_A, x_B, ξ_A, ξ_B, $\Delta M_A^{id,tm}$, $\Delta M_B^{id,tm}$, $\Delta R_A^{id,tm}$, $\Delta R_B^{id,tm}$, $\Delta \rho_{un}^{tm}$ and $\Delta \rho_{cr}^{tm}$ by $S_{un}^x(t_2)$, $x_A(t_1)$, $x_B(t_1)$, $\xi_A(t_1)$, $\xi_B(t_1)$, $\Delta M_A^{id,tm}(t_2)$, $\Delta M_B^{id,tm}(t_2)$, $\Delta R_A^{id,tm}(t_2)$, $\Delta R_B^{id,tm}(t_2)$, $\Delta \rho_{un}^{tm}(t_2)$ and $\Delta \rho_{cr}^{tm}(t_2)$ respectively.

The stress, $\sigma_{un}^t(t_2)$ at time t_2 may be expressed from Eq. (23) on using Eq. (12) as

$$\sigma_{un}^t(t_2) = \Delta \sigma_{un}^{it}(t_1) + E_c(t_2) \left[\Delta \varepsilon_{un}^{tm}(t_2) - \alpha T_1 \right]$$

$$+ E_e(t_2, t_1) \left\{ \Delta \varepsilon_{un}^{it}(t_1) \left[\lambda_{un}^c(t_2, t_1) - \phi(t_2, t_1) \right] + \Delta \varepsilon_{un}^s(t_2, t_1) - \varepsilon^{sh}(t_2, t_1) \right\}$$

$$- E_e(t_1, t_1) \left\{ \Delta \varepsilon_{un}^{it}(t_1) \left[\lambda_{un}^c(t_1, t_1) - \phi(t_1, t_1) \right] + \Delta \varepsilon_{un}^s(t_1, t_1) - \varepsilon^{sh}(t_1, t_1) \right\}$$

$$+ \Delta \sigma_{un}^{id,cs}(t_2) + \Delta \sigma_{un}^{id,tm}(t_2) \tag{61}$$

Further, on using Eq. (8) for evaluation of $\Delta \varepsilon_{un}^{it}(t_1)$, noting that $\lambda_{un}^c(t_1, t_1)$, $\Delta \varepsilon_{un}^s(t_1, t_1)$, $\varepsilon^{sh}(t_1, t_1)$ and $\phi(t_1, t_1)$ are equal to zero and rearranging the terms, Eq. (61) may be expressed in the same form as Eq. (28), on replacing the terms in parentheses t_1 by t_2, where the coefficients $a(t_2)$, $b(t_2)$ and $c(t_2)$ are given as

$$a(t_2) = -0.5 \, S_{un}^{xy}(t_1) w \left[E_c(t_1) + E_e(t_2, t_1) q(t_2, t_1) \right] \tag{62}$$

$$b(t_2) = S_{un}^{xy}(t_1) \Delta R_A^{it}(t_1) \left[E_c(t_1) + E_e(t_2, t_1) q(t_2, t_1) \right] + S_{e,un}^{xy}(t_2, t_1) \Delta R_A^{id,cs}(t_2) E_e(t_2, t_1)$$

$$+ S_{un}^{xy}(t_2) \Delta R_A^{id,tm}(t_2) E_c(t_2) \tag{63}$$

$$c(t_2) = -S_{un}^{xy}(t_1) \Delta M_A^{it}(t_1) \left[E_c(t_1) + E_e(t_2, t_1) q(t_2, t_1) \right] - S_{e,un}^{xy}(t_2, t_1) \Delta M_A^{id,cs}(t_2) E_e(t_2, t_1)$$

$$- S_{un}^{xy}(t_2) \Delta M_A^{id,tm}(t_2) E_c(t_2) + E_e(t_2, t_1) r(t_2, t_1) + E_c(t_2) s(t_2) \tag{64}$$

where $q(t_2, t_1) = \lambda_{un}^c(t_2, t_1) - \phi(t_2, t_1)$; $r(t_2, t_1) = \Delta\varepsilon_{un}^s(t_2, t_1) - \varepsilon^{sh}(t_2, t_1)$; $s(t_2) = \Delta\varepsilon_{un}^{tm}(t_2) - \alpha T_1$

The crack lengths $x_A(t_2)$ and $x_B(t_2)$ and the coefficients $\xi_A(t_2)$ and $\xi_B(t_2)$ at time t_2 are now obtained from Eqs. (53)-(56) respectively on replacing the terms in the parentheses t_1 by t_2 and replacing κ by 0.5 in Eqs. (55) and (56).

Now consider the second time interval(t_2, t_3). In addition to the two forces, $\Delta M^{it}(t_1)$ generated at time t_1 and $\Delta M^{id,cs}(t_2)$ generated at time t_2, a force $\Delta M^{it}(t_2)$ that results from change in crack lengths in the previous time interval(t_1, t_2) needs to be considered in this time interval(t_2, t_3). Thus creep in this interval is caused due to one force $\left[\Delta M^{it}(t_1)\right]$ generated at time t_1 and two forces $\left[\Delta M^{it}(t_2),\ \Delta M^{id,cs}(t_2)\right]$ generated at time t_2 (Fig. 6). It may be noted that the force $\Delta M^{id,tm}(t_2)$ is considered not to cause creep subsequently, since as stated earlier in the section 2, the thermal gradients are superimposed only at an instant of time. The bending moment, $\Delta M^{it}(t_2)$ is obtained by carrying out a displacement analysis for which the fixed end force vector is taken equal to the change in fixed end forces owing to change in the crack lengths.

Further analysis proceeds in the similar manner as explained for the first time interval. In the ith time interval (t_i, t_{i+1}), there are $1 + 2(i-1)$ number of moments causing creep as shown in Fig. 6. The creep effect of $1 + 2(i-1)$ number of moments, the shrinkage effect and the thermal gradient effect can be evaluated in a similar manner as explained for the first time interval. The total midspan deflections and the stresses can be expressed in a form similar to Eqs. (60) and (61) respectively.

The number of time intervals is decided on the criteria that the change in the values of moments, M and mid-span deflections, d_m for any span, with increase in number of time intervals, should not be more than 1%.

5   Validation and numerical study

In order to validate the proposed procedure, first, the results have been compared with the experimental and analytical results reported by Gilbert and Bradford [18] for two two-span continuous composite beams B1, B2 with each span 5.8 m long. The beam B1 was subjected to a superimposed uniformly distributed span load (w) of 4.45 kN/m in addition to the dead load (1.92 kN/m) whereas beam B2 was subjected to dead load only. The beams were tested for a period of 340 days ($\phi = 1.68$, $\varepsilon^{sh} = 0.00052$) and the mid-span deflections of beams were measured during the test. The cross-section [Fig. 2(a)] of the composite beams consisted of a steel section (203×133UB 25) and a concrete slab ($b_c = 1000$ mm; $D_c = 70$ mm; $A_{sr} = 113\,mm^2$; $D_{sr} = 15$ mm). The properties of concrete at 28 days were: $E_c = 2.20 \times 10^4 N/mm^2$; f_t= -3.0 N/mm^2 and for steel $E_s = 2.0 \times 10^5 N/mm^2$. The values of ϕ and ε^{sh} are assumed to vary with time in accordance with the provisions of CEB-FIP MC 90 [12].

The values of total mid-span deflections, $d_m^t(t)$obtained from the proposed procedure are in reasonable agreement with the reported experimental values of mid-span deflections (Fig. 7). The values of $d_m^t(t)$ obtained from the proposed procedure for both the beams are lower than

the analytical values reported by Gilbert and Bradford [18]. The higher values of analytical procedure can be ascribed to: (1) neglect of tension stiffening, (2) neglect of creep effect of $\Delta M^{id,cs}$ and (3) the manner in which the crack length is established i.e. the same crack length is assumed for the entire time interval which begins from the time of application of load. Therefore two more sets of results are obtained from the proposed procedure: (1) neglecting tension stiffening and considering creep effect of $\Delta M^{id,cs}$ and (2) neglecting both tension stiffening and creep effect of $\Delta M^{id,cs}$. These results are also shown in Fig. 7. As expected, the values obtained from the proposed procedure now are closer to the analytical results.
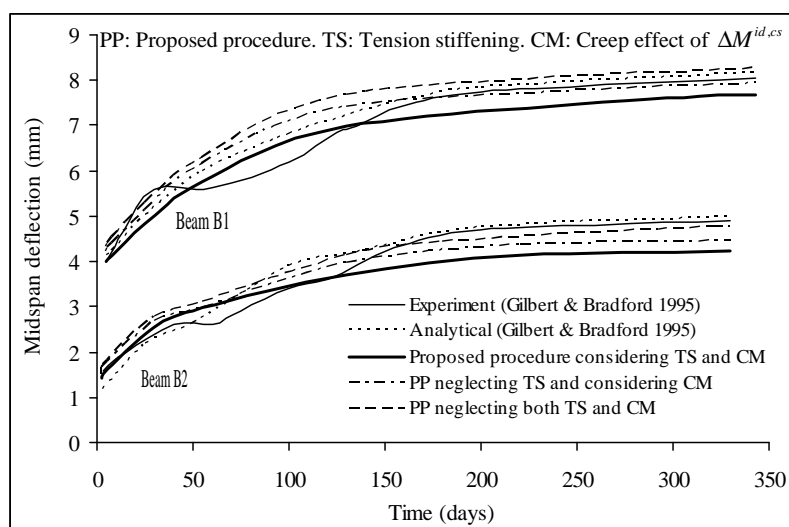
Figure 7: Comparison of mid-span deflections of beams B1 and B2.

Next, the results obtained from the proposed procedure have been validated by comparison with those obtained from a general purpose finite element program, $ABAQUS$ [20], for a three span continuous beam of a composite bridge designated as beam B3 [Fig. 8(a)]. The cross-section [Fig. 2(a)] of the beam consists of a concrete slab ($b_c = 1000$ mm; $D_c = 200$ mm; $A_{sr} = 471\,mm^2$; $D_{sr} = 30$ mm) and a 1100 mm deep steel I section having second moment of area, $1.34 \times 10^{10}\,mm^4$ about its centroid and $A_{ss} = 65500\,mm^2$. The properties of concrete at 28 days are: $E_c = 3.35 \times 10^4 N/mm^2$; f_t= -3.4 N/mm^2 and for steel $E_s = 2.0 \times 10^5 N/mm^2$.

Two types of meshes, fine and coarse have been considered. The fine mesh (Fig. 9) for the entire composite beam consists of 640(160×4) shell elements (S4R elements) and 160 beam elements (B31OS elements) whereas the coarse mesh consists of 160(80×2) S4R elements and 80 B31OS elements. The condition of no slip between the slab and the steel section is achieved by using multipoint constraints (MPC'S), of type BEAM, between corresponding shell and beam elements. Creep of the concrete is taken into account by modeling concrete as viscoelastic material in time domain whereas shrinkage is taken into account by applying equivalent temperature

loading (temperature and coefficient of thermal expansion are assumed to vary in such a manner that the thermal strain of concrete at any instant of time is equal to ε^{sh}). Considering the fact that the viscoelastic material model cannot be combined with the cracking [24] in *ABAQUS* and also that the thermal gradient is assumed to act at an instant of time, three types of analyses have been considered: (1) instantaneous analysis considering cracking only (2) analysis considering the thermal gradient only, (2) time-dependent analysis for 10,000 days considering creep and shrinkage and neglecting cracking and the thermal gradient. For all three analyses, w=40 kN/m is considered. In analysis 1 and 2, w is assumed to be applied at 3 days whereas in analysis 3, w is assumed to be applied at 28 days. In analysis 2, a thermal gradient is assumed to act at 4 days and a trilinear temperature profile corresponding to the negative temperature gradient suggested by AASHTO [1] for zone 3 [Fig. 2(b)] is considered, where $T_1 = -9\,^0$C, $g_1 = 0.066\,^0$C/mm, $g_2 = 0.0078\,^0$C/mm. The values of coefficients of thermal expansion, α_c and α_s in this analysis (analysis 2) are assumed to be as 10×10^{-6} mm/mm/ ^{0}C. For analysis 3, ϕ and ε^{sh} are assumed to be 2.15 and 0.00043 respectively at 10,000 days and the values of ϕ and ε^{sh} are assumed to vary with time in accordance with the provisions of CEB-FIP MC 90 [12].
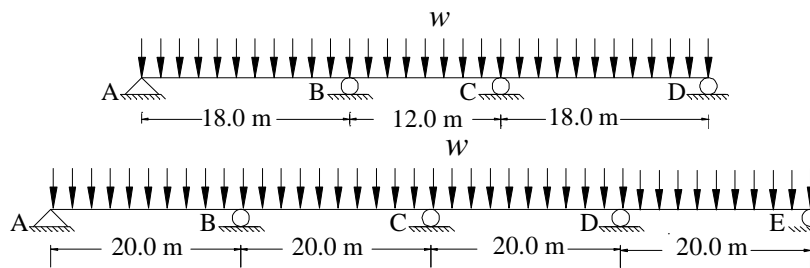
Figure 8: Longitudinal profile of beams: (a) beam B3; and (b) beam B4.
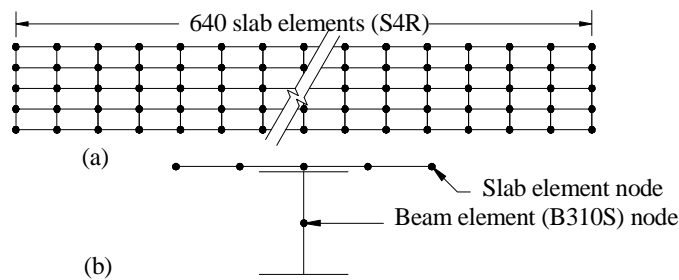
Figure 9: Finite elements mesh for beam B3: (a) shell elements in slab; and (b) nodes in the cross section.

Consider analysis 1. The values of bending moment, M^{it} (3) at support B (or C), are obtained as 988.02 kN-m and 986.40 kN-m using fine and coarse meshes respectively. The

values of midspan deflection, $d_m^{it}(3)$ of span AB (or CD), which is of design importance, are obtained as 8.72 mm and 8.78 mm using fine and coarse meshes respectively. The fine mesh is therefore adequate and is considered for validation.

The results from the proposed procedure and ABAQUS (fine mesh) for all three analyses are compared in Table 1 and it is observed that for all three analyses, the results obtained from the proposed procedure are in reasonable agreement with the results obtained from *ABAQUS*. Major portions of the differences between the results may be due to the consideration of biaxial state of stress in *ABAQUS* and due to introduction of MPC's (type BEAM) between only one node each of adjacent shell elements and a beam element (only available nodes for the connection in the chosen finite element model) across a cross-section. Further, in analysis 3, some difference would also result from choice of the same value of χ for creep and shrinkage. However, this difference is likely to be small.

Table 1: Comparison of results of proposed procedure and ABAQUS for beam B3.

Analysis	Moment at support B (kN-m)			Midspan deflection of span AB (mm)		
	Proposed Procedure	Abaqus	% difference	Proposed Procedure	Abaqus	% difference
1 $M^{it}(3), d_m^{it}(3)$	1002.25	988.02	1.44	8.09	8.72	7.22
2 $M^{t}(4), d_m^{t}(4)$	1128.44	1102.25	2.38	7.99	8.65	7.63
3 $M^{t}(10000), d_m^{t}(10000)$	1674.21	1699.04	1.46	11.79	12.55	6.06

It may be noted that the total number of degrees of freedom for the beam B3 is 5957 for *ABAQUS* whereas the corresponding number of total degrees of freedom for the proposed procedure is 12. Therefore, the computational effort required for the proposed procedure is a very small fraction of that required for the finite element analysis.

Further numerical studies have also been carried out for a four span continuous beam of a composite bridge designated as beam B4 [Fig. 8(b)]. The cross-section [Fig. 2(a)] and material properties are same as those of beam B3. The uniformly distributed load, w, on the beams has been taken as two times, three times and four times the cracking load, $w_{cr}(= 14.2$ kN/m for loading at three days), the load at which cracking first takes place at a support (supports B and D) of the beam. Three analyses have been carried out for each loading: (1) instantaneous analysis at 3 days neglecting cracking, (2) instantaneous analysis at 3 days considering cracking and (3) time-dependent analysis for 10,000 days (ϕ=2.15; ε^{sh}=0.00043) considering creep, shrinkage and thermal gradient. Again AASHTO [1] zone 3 negative thermal gradient is considered. The negative thermal gradient is chosen since this results in additional cracking. Taking into account

the symmetry of the beam, moments for supports B and C along with mid-span deflection of spans AB and BC have been presented in Table 2.

Table 2: Results of numerical studies for beam B4.

| w/w_{cr} | Analysis | $M^{it}(3), M^{t}(10000)$ (kN-m) | | $d_m^{it}(3), d_m^{t}(10000)$ (mm) | |
| | | Support | | Span | |
		B	C	AB	BC
2	1	1217.14	811.43	6.69	1.97
	2	1144.29	828.69	7.07	2.23
	3	1625.13	1143.35	13.13	3.68
3	1	1825.71	1217.14	10.03	2.95
	2	1663.84	1218.41	10.86	3.68
	3	2210.49	1614.12	18.00	5.48
4	1	2434.29	1622.86	13.38	3.94
	2	2184.47	1601.96	14.63	5.14
	3	2795.34	2039.40	22.83	7.16

Consider the effect of cracking (i.e. change from analysis 1 to analysis 2) on instantaneous moments and midspan deflections. It can be observed from the results that due to cracking, the instantaneous moment, $M^{it}(3)$ at support B, reduces by up to 10.26% (for $w/w_{cr} = 4$) whereas $M^{it}(3)$ at support C increases (for $w/w_{cr} = 2, 3$) owing to relatively larger cracking at its adjacent supports (support B and D) in comparison to cracking at support C. The increase in instantaneous mid-span deflection, $d_m^{it}(3)$ of span BC due to cracking of concrete is up to 30.46% (for $w/w_{cr} = 4$).

Consider now the effect of creep, shrinkage and thermal gradient (i.e change from analysis 2 to analysis 3) on bending moments and midspan deflections. The increase in $M^{it}(3)$ at support B is up to 42.02% (for $w/w_{cr} = 2$) and the increase in $d_m^{it}(3)$ of span AB due is up to 85.72% (for $w/w_{cr} = 2$).

It may be further noted that the number of time intervals required for convergence of total bending moments and total mid-span deflections, within 1% is less than 20 for all the cases considered for the validation and the numerical study.

6 Conclusions

A hybrid analytical-numerical procedure has been presented in this paper for continuous composite bridges subjected to service load. The procedure takes into account the effects of concrete

cracking, creep and shrinkage in the concrete portion and the thermal gradient across the cross section of the continuous composite bridges. The procedure is analytical at the elemental level and numerical at the structural level. Closed form expressions for the stiffness matrix, end displacements, crack lengths, interpolation coefficients, and the mid-span deflection of the cracked span length beam element have been presented. The results obtained from the proposed procedure are found to be in reasonable agreement with the experimental, analytical and finite element results. The computational effort required by the proposed procedure is shown to be a small fraction of that required for finite element analysis. It is observed that the instantaneous moment at a support may increase due to much larger cracking at adjacent supports. The proposed procedure can be readily extended for the analysis of composite integral bridges and three dimensional framed buildings.

References

[1] AASHTO. *AASHTO LRFD bridge design specifications.* American Association of State Highway and Transportation Officials, Washington (DC), 1998.

[2] C. Amadio and M. Fragiacomo. Simplified approach to evaluate creep and shrinkage effects in steel-concrete composite beams. *Journal of Structural Engineering, ASCE*, 123(9):1153–1162, 1997.

[3] M. Arockiasamy and M. Sivakumar. Time dependent behaviour of continuous composite integral abutment bridges. *Practice Periodical on Structural Design and Construction, ASCE*, 10(3):161–170, 2005.

[4] Z. P. Bazant. Prediction of concrete creep effects using age-adjusted effective modulus method. *ACI Journal*, 69(4):212–217, 1972.

[5] M. A. Bradford and R. I. Gilbert. Experiments on composite tee-beams at service loads. *Civil Engineering Transactions*, CE33(4):285–291, 1991.

[6] M. A. Bradford and R. I. Gilbert. Composite beams with partial interaction under service loads. *Journal of Structural Engineering, ASCE*, 118(7):1871–1883, 1992.

[7] M. A. Bradford, H. Vu. Manh, and R. I. Gilbert. Numerical analysis of continuous composite beams under service loading. *Advances in Structural Engineering*, 5(1):1–12, 2002.

[8] D. Cusson and W. L. Repette. Early-age cracking in reconstructed concrete bridge barrier walls. *ACI Materials Journal*, 97(4):438–446, 2000.

[9] L. Dezi, G. Leoni, and A. M. Tarantino. Time-dependent analysis of prestressed composite beams. *Journal of Structural Engineering, ASCE*, 121(4):621–633, 1995.

[10] L. Dezi, G. Leoni, and A. M. Tarantino. Algebraic methods for creep analysis of continuous composite beams. *Journal of Structural Engineering, ASCE,*, 122(4):423–30, 1996.

[11] L. Dezi and A. M. Tarantino. Creep in composite continuous beams. i: Theoretical treatment. *Journal of Structural Engineering, ASCE*, 119(7):2095–2111, 1993.

[12] Comite' Euro International du Beton-Fe'de'ration International de la Pre'contrainte. Ceb-fip model code 1990 for concrete structures. *Bulletin d' information No. 213/214, Laussane(Switzerland)*, 1993.

[13] M. Elbadry, S. Youakim, and A. Ghali. Model analysis of time-dependent stresses and deformations of structural concrete. *Progress in Structural Engineering and Materials*, 5(3):153–166, 2003.

[14] European Committee for Standardization. *Eurocode 2: Design of Concrete Structures, Part 1: General rules and rules for buildings.* Brussels, Belgium, 1992.

[15] M. Fragiacomo, C. Amadio, and L. Macorini. Finite-element model for collapse and long-term analysis of steel-concrete composite beams. *Journal of Structural Engineering, ASCE*, 130(3):489–497, 2004.

[16] A. Ghali, R. Favre, and M. Elbadry. *Concrete Structures: Stresses and Deformations.* Spon Press, London, 2002.

[17] R. I. Gilbert. *Time effects in concrete structures.* Elsevier, Amsterdam, 1998.

[18] R. I. Gilbert and M. A. Bradford. Time-dependent behavior of continuous composite beams at service loads. *Journal of Structural Engineering, ASCE*, 121(2):319–327, 1995.

[19] R. Hadidi, M. A. Saadeghvaziri, and C. T. T. Hsu. Practical tool to accurately estimate tensile stresses in concrete bridge decks to control transverse cracking. *Practice Periodical on Structural Design and Construction, ASCE*, 8(2):74–82, 2003.

[20] Abaqus/standard, version 6.1. inc. Pawtucket (RI, USA), 2001.

[21] H. G. Kwak and Y. J. Seo. Long-term behavior of composite girder bridges. *Computers and Structures*, 74(5):583–599, 2000.

[22] H. G. Kwak, Y. J. Seo, and C. M. Jung. Effect of slab casting sequences and the drying shrinkage of concrete slabs on the short-term and long-term behaviour of composite steel box girder bridges. part 1. *Engineering Structures*, 23(11):1453–1466, 2000.

[23] H. G. Kwak, Y. J. Seo, and C. M. Jung. Effect of slab casting sequences and the drying shrinkage of concrete slabs on the short-term and long-term behaviour of composite steel box girder bridges. part 2. *Engineering Structures*, 23(11):1467–1480, 2000.

[24] L. Macorini, M. Fragiacomo, C. Amadio, and B. A. Izzuddin. Long-term analysis of steel-concrete composite beams: Fe modeling for effective width evaluation. *Engineering Structures*, 28(11):1110–1121, 2006.

[25] A. Mari, E. Mirambell, and I. Estrada. Effect of construction process and slab prestressing on the serviceability behavior of composite bridges. *Journal of Constructional Steel Research*, 59(2):135–163, 2003.

[26] D. J. Ohelers and M. A. Bradford. *Elementary behaviour of composite steel and concrete structural members.* Butterworth-Heinemann, Oxford, 1999.

[27] M. Sakr and J. Lapos. Time-dependent analysis of partially prestressed continuous composite beams. In *In Proceedings of Second International PhD Symposium in Civil Engineering*, Budapest, 1998.

[28] H. K. Thippeswamy, H. V. S. Gnagarao, and J. M. Franco. Performance evaluation of jointless bridges. *Journal of Bridge Engineering, ASCE*, 7(5):276–289, 2002.